Available online at www.sciencedirect.com
ScienceDirect
Journal of Photochemistry and Photobiology A: Chemistry 188 (2007) 364–370
Journal of Photochemistry and Photobiology A:Chemistry
www.elsevier.com/locate/jphotochem

Hybrid solar cells with ordered TiO_2 nanostructures and MEH-PPV

Seok-Soon Kim, Jang Jo, Chaemin Chun, Jae-Chul Hong, Dong-Yu Kim *

Heeger Center for Advanced Materials, Department of Materials Science and Engineering, Gwangju Institute of Science and Technology (GIST), Gwangju 500-712, South Korea

Received 20 September 2006; received in revised form 19 December 2006; accepted 27 December 2006
Available online 29 December 2006

Abstract

For use in hybrid solar cells consisting of TiO_2 and poly[2-methoxy, 5-(2′-ethyl-hexyloxy)-1,4-phenylenevinylene] (MEH-PPV), a TiO_2 nanostructure which has periodic hexagonal hole arrays was fabricated using surface relief gratings on azobenzene-functionalized polymer films as a template in the sol–gel reaction of a Ti-precusor. The ordered bulk heterojunction solar cells, prepared with the TiO_2 nanostructure and MEH-PPV, have a higher power conversion efficiency of 0.21% compared to bilayer and random bulk heterojunction solar cells fabricated with thin-dense TiO_2 films and randomly networked TiO_2 nanoparticles, respectively, under one sun with air mass 1.5 global illumination.

Keywords: Hybrid solar cells; TiO_2 nanostructure; Surface relief gratings

1. Introduction

Polymer organic solar cells based on an interpenetrating network of electron donors and acceptors prepared using solutions of conjugated polymers have become attractive for use in inexpensive large area and low weight devices [1–7]. Although power conversion efficiencies of 4–5% have been reported in recent years, for practical applications, several factors that limit efficiency, including the poor stability of the active layer under the illumination, poor overlap between the absorption spectrum of the polymer and the solar spectrum, phase segregation, and the low mobility of charge carriers, particularly electrons, must be overcome [8–11]. One potential solution is the application of inorganic nanoparticles or nanostructures such as nanorods and nanowires as electron acceptors, to utilize the high electron mobility of the inorganic phase [12–29].

Typically, nanocrystalline TiO_2, which is the most promising material due to its chemical stability, easy control of size and shape, proper band gap, and low cost, is prepared on a conducting substrate by casting or a sol–gel method followed by heat-treatment to achieve electrical networking for efficient electron transport. The TiO_2 nanocrystalline electrode is then filled with a conjugated polymer such as poly[2-methoxy, 5-(2′-ethyl-hexyloxy)-1,4-phenylenevinylene] (MEH-PPV) [14,18,19]. In this case, randomly networked TiO_2 nanoparticles can cause poor charge transport and the infiltration of conjugated polymers is difficult, due to the nanosized pore distribution. Although the blending of inorganic nanocrystals with conjugated polymers also can be used in the fabrication of hybrid solar cells, finding a proper solvent that accommodates both inorganic nanostructures and conjugated polymers is a serious problem in terms of obtaining sufficient efficiency for the commercialization of hybrid solar cells [22]. To overcome these problems new approaches such as application of ordered inorganic nanostructures and the use of a molecular precursor for inorganic semiconductor have recently been reported [17,20,22,23]. In addition, increased efficiencies were reported by improving morphology of the TiO_2 layer, which was fabricated using polystylene-*block*-polyethylene oxide diblock copolymer template, and by introducing a poly(ethylenedioxythiophene)/polystylene sulphonate as the hole collector between active layer and metal electrode [26–29].

In this work, we report on the fabrication of an ordered bulk heterojunction organic–inorganic hybrid solar cell using well-ordered nanostructures of TiO_2 and poly[2-methoxy, 5-(2′-ethyl-hexyloxy)-1,4-phenylenevinylene] (MEH-PPV) as the electron acceptor and donor, respectively. Well-ordered nanostructures of TiO_2 which containing periodic hexagonal hole arrays were fabricated by a simple, controllable, economical and reproducible method, using 2D surface relief gratings (SRGs)

* Corresponding author. Tel.: +82 62 970 2319; fax: +82 62 970 2304.
E-mail address: kimdy@gist.ac.kr (D.-Y. Kim).

1010-6030/$ – see front matter © 2007 Elsevier B.V. All rights reserved.
doi:10.1016/j.jphotochem.2006.12.037

on polymer films as a template during the spin-on based sol–gel process of a Ti-precusor. Optical fabrication of surface relief gratings (SRGs) on azobenzene-functionalized polymer films has significant advantages including a one-step process, controllability of grating profiles, reversibility and the capability of superimposing multiple patterns on the same spot [30–34]. In a one-step process of exposure to an appropriate interference pattern of light, sinusoidal SRGs could be formed on azobenzene-functionalized polymer films as the result of mass transport of the polymer chain.

For comparison with ordered hybrid solar cells fabricated from these nanostructures, two types of TiO_2 acceptors, randomly networked nanoparticles and thin-dense films, were also prepared and applied to the fabrication hybrid solar cells.

2. Experimental section

All chemicals were purchased from Aldrich. ITO (Samsung Corning Co., Ltd.) coated glass substrates were cleaned by ultrasonication with an organic solvent and Millopore water followed by drying in a stream of N_2. Poly (disperse orange 3) (PDO3), an azo-functionalized polymer, was synthesized from the diglycidyl ether of bisphenol A and disperse orange 3 following the literature procedure, and reprecipitated using tetrahydrofuran and methanol [35]. PDO3 films were prepared using 10 wt.% PDO3 in cyclohexanone by a spin coating process followed by drying in a vacuum oven at 100 °C. 2D SRGs on PDO3 films were formed by a two step exposure to an interference pattern of Ar^+ laser beams at a wavelength of 488 nm with an intensity of 80 mW/cm^2 with a rotation angle of 60° [34]. 0.5 ml of Ti-isopropoxide in 20 ml of 2-propanol containing 0.8 ml of HCl was used as the Ti-precusor for the sol–gel reaction with SRG templates at room temperature. The formation of 2D SRGs and the TiO_2 nanostructure with a hexagonal hole array was confirmed by atomic force microscopy (AFM, Autoprobe CP, PSI) and scanning electron microscopy (SEM, Hitachi S-4700), respectively.

Optical properties of the MEH-PPV and TiO_2 nanostructures with MEH-PPV were investigated via UV/vis absorption spectral measurements and photoluminescence (PL) spectral measurements.

To characterize the photovoltaic properties, three types of organic–inorganic hybrid solar cells were fabricated. Flat TiO_2 film and ordered TiO_2 nanostructure based devices were prepared by a spin-on based sol–gel reaction without and with 2D SRGs as templates, respectively. The conventional type of electron acceptors, consisting of random networks of sintered TiO_2 nanoparticles, was also prepared by the spin coating of a colloidal suspension of TiO_2 followed by sintering at 425 °C. MEH-PPV which acts as an absorber of light and an electron donor was prepared on the TiO_2 electrodes by spin coating a 0.8 wt.% solution in chlorobenzene followed by baking at 50 °C. Finally, a Au top electrode was evaporated thermally in a vacuum at a pressure of the order of 10^{-6} Torr.

Cell performance was measured under one sun using a xenon light source and an air mass (AM) 1.5 global filter. Photocurrent–voltage (*I–V*) measurements were performed using an Autolab PGSTAT30 Potentiostat/Galvanostat.

3. Results and discussion

As shown in Fig. 1, the process used in the fabrication of ordered hybrid solar cells with TiO_2 nanostructures as an electron acceptor started with the preparation of an azobenzene-functionalized polymer film on a thin TiO_2 blocking layer, prepared to restrict recombination resulted from the direct contact of ITO and MEH-PPV. The thin TiO_2 blocking layer was prepared on ITO by spin-coating of a Ti-precusor solution followed by sintering at 425 °C for 1 h and PDO3 was spun on this thin TiO_2 blocking layer and dried at 100 °C to remove residual solvent.

SRGs were fabricated on the PDO3 polymer film, which has the chemical structure shown in Fig. 2(b), using an interference pattern of an Ar^+ laser beam at 488 nm with an intensity of 80 mW/cm^2 with the holographic optical set-up shown in Fig. 2(a). The linearly polarized light of the Ar^+ laser beam was passed through a half-wave plate to achieve a p-polarized state and then expanded and collimated through a spatial filter and a lens. About half of the collimated beam was directly incident on the film and other portion was reflected on the film by an aluminium-coated mirror [30,31].

To obtain hexagonal type 2D SRGs, after the formation of 1D SRGs (Fig. 1(b)), the substrate was then rotated by 60° around its normal axis followed by a second exposure (Fig. 1(c)). Using these 2D SRGs as templates in the spin-on based sol–gel reaction of a Ti–precusor solution followed by heat-treatment, TiO_2 nanostructures with periodic hexagonal hole arrays were produced (Fig. 1(d)).

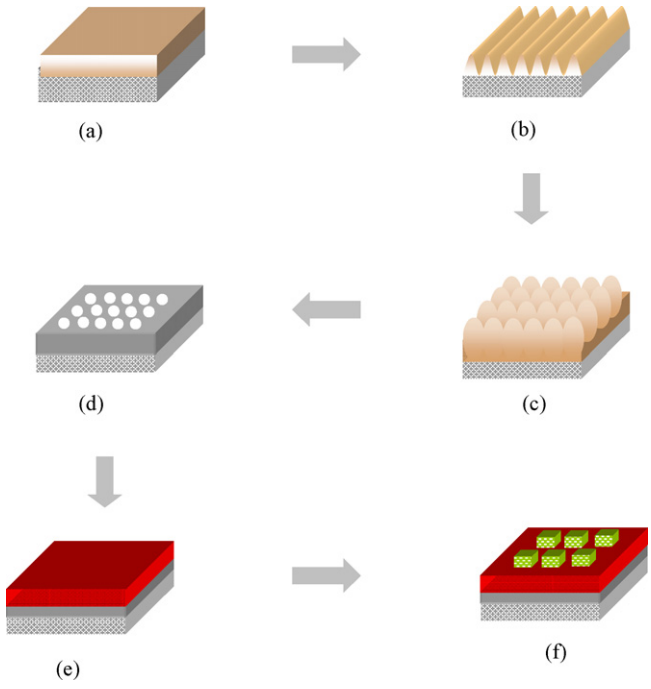

Fig. 1. Schematic representation of the fabrication of TiO_2 nanostructures and MEH-PPV hybrid solar cells.

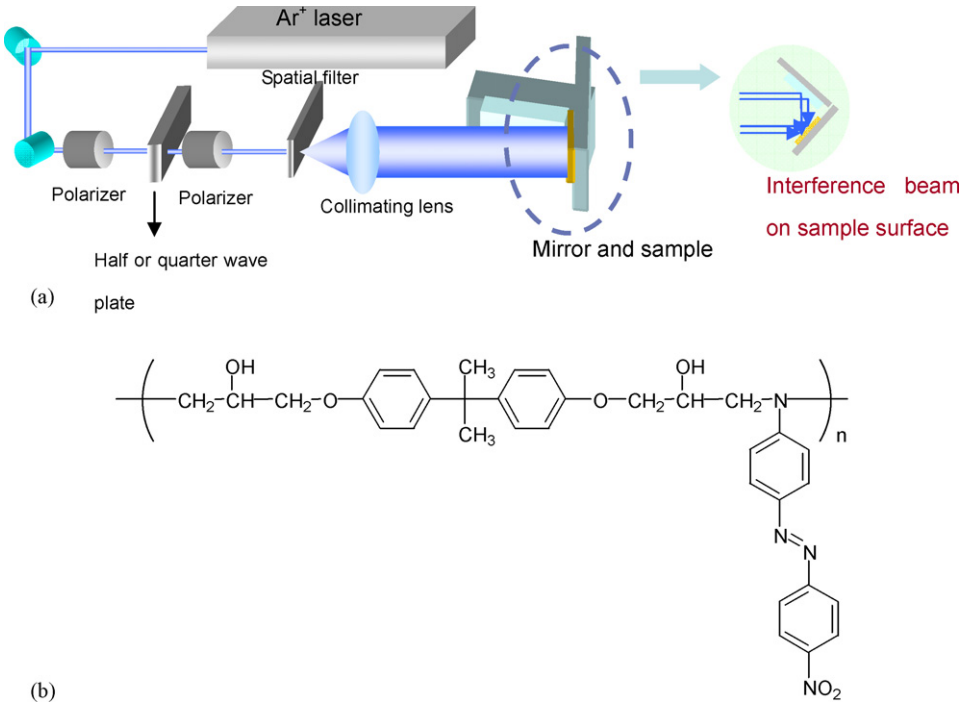

Fig. 2. (a) Experimental set-up for the formation of surface relief grating and (b) chemical structures of PDO3.

When a drop of Ti isopropoxide in 2-propanol containing HCl was placed on the SRGs and spun, the precursor was converted to amorphous TiO_2 by hydrolysis. The spin-coated material was heat treated for 12 h in several steps (room temperature → 100 → 400 → 425 °C) to remove the polymer template and to produce crack-free crystalline TiO_2. The HCl was added to the sol solution, in this case, to slow down and control the rate of hydrolysis of Ti isopropoxide [36]. Here, the size and distance of the periodic holes and the thickness of TiO_2 can be tuned by controlling the precursor concentration, the spin-rate, and the depth and period of the SRGs. The fabrication of hybrid solar cells was completed by spin-coating MEH-PPV solutions followed by the thermal evaporation of Au as shown in Fig. 1(e) and (f).

When PDO3 is coated on the thin TiO_2 blocking layer, it has a smooth surface, similar to other types of polymer films (shown in Fig. 3(a)). By exposing this smooth polymer film to the interference beam using the optical set-up shown in Fig. 2(a), the SRGs are formed on the polymer films. Fig. 3(b) shows SRGs formed on a polymer film which have a 500 and ∼100 nm spacing and depth, respectively, and the successful formation of 2D hexagonal SRGs after a second exposure with a 60° rotation was confirmed by the AFM images shown in Fig. 3(c). Using 2D SRGs as a template in the sol–gel reaction of the Ti-precusor, a 2D TiO_2 nanostructure which has periodic hexagonl hole arrays was produced.

Fig. 4(a) shows SEM images of 2D TiO_2 nanostructure with periodic hole arrays with a spacing of 500 nm and a diameter of ∼90 nm. When the Ti-precusor was spun on the 2D SRGs, the solution is gathered in the groove and converted to the amorphous TiO_2. On heat-treating this sample, the residual PDO3 is removed and periodic holes are generated in the position of the hill of the 2D SRGs due to the selective formation of TiO_2 during the spin-on based sol–gel reaction. A peak at ∼4.5 keV corresponding to the Ti Ka 1 in the EDX spectra of the TiO_2 nanostructure verified the successful formation of a TiO_2 and the complete elimination of the SRG polymer template (shown in Fig. 4(b)).

Before the fabrication and characterization of solar cells, the optical properties of MEH-PPV, TiO_2, and MEH-PPV incorporated TiO_2 nanostructures were investigated. Fig. 5 shows absorption and PL spectra of MEH-PPV and TiO_2/MEH-PPV hybrid films. The absorption spectra of MEH-PPV in Fig. 5(a) with an absorption peak at 500 nm, attributed to the $\pi \rightarrow \pi^*$ transition, is consistent with the previously reported results and the spectrum of TiO_2/MEH-PPV is apparently formed of the two component contribution and no wavelength shift is observed, compared to the absorption of a pure MEH-PPV film [37]. This indicates that ground-state charge transfer at the interfaces is negligible [38]. The PL emission of MEH-PPV under excitation at 500 nm is also consistent with other reports and a significant quenching of the emission intensity resulting from the infiltration of MEH-PPV into the TiO_2 nanostructures can be observed in Fig. 5(b). This indicates the efficient charge separation at the TiO_2/MEH-PPV interface, which results in the production of electricity under illumination by light.

To characterize the solar cells consisting of TiO_2 and MEH-PPV as an electron acceptor and donor, respectively, three types of TiO_2 electron acceptors with same thickness of ∼100 nm were prepared. Fig. 6 shows the surface morphology of the three types of TiO_2 electrodes, a random network of sintered TiO_2 nanoparticles, a flat-dense TiO_2 film, and 2D ordered TiO_2 nanostructures fabricated by the process shown in Fig. 1. A porous TiO_2 electrode, used in the fabrication of typical hybrid

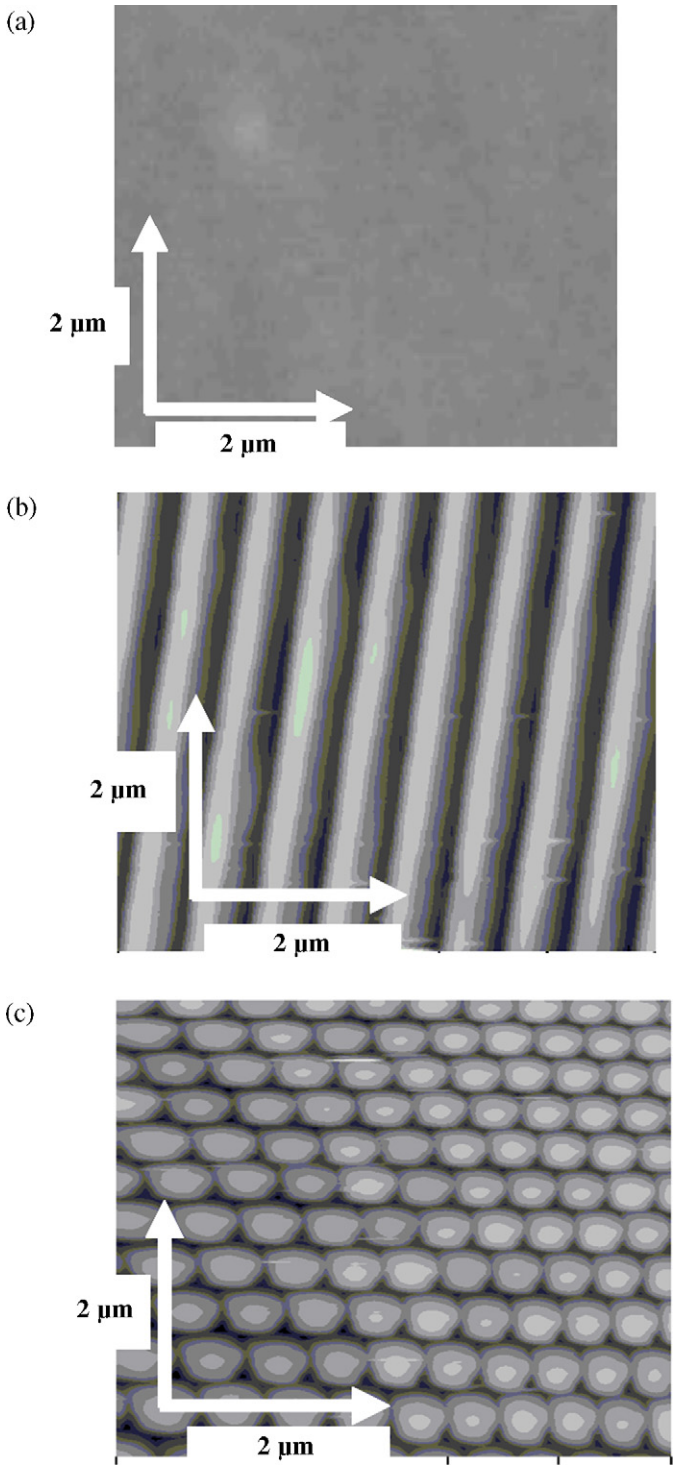

Fig. 3. AFM images and of (a) a PDO3 polymer film, (b) 1D SRGs on a polymer film, and (c) 2D hexagonal SRGs on a polymer film.

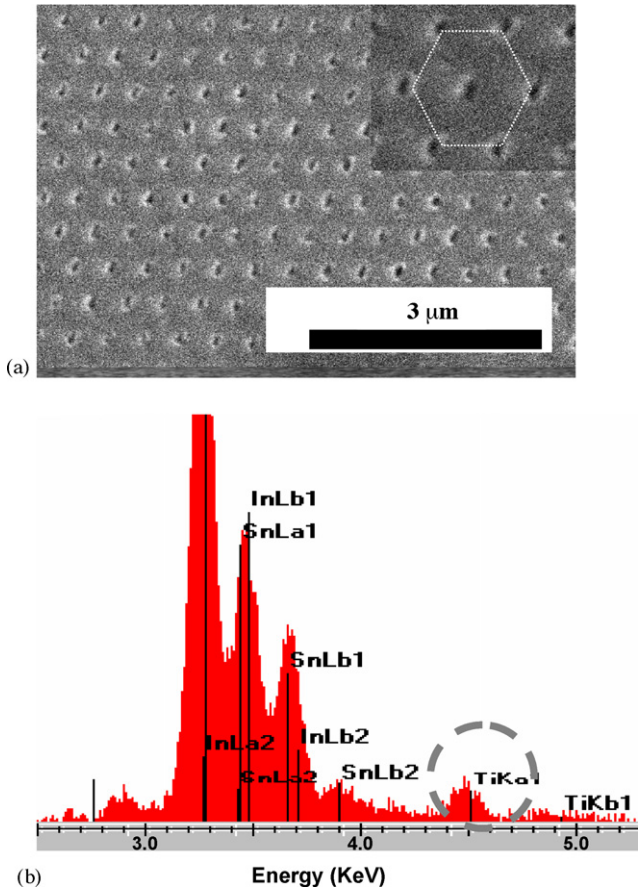

Fig. 4. (a) SEM images and (b) EDX spectra of a TiO_2 nanostructure with a hexagonal array of periodic holes, prepared using 2D SRGs as templates.

solar cells, was fabricated by spin-coating of a colloidal suspension of TiO_2 nanoparticles followed by sintering at ~425 °C and the formation of porous structure can be confirmed in Fig. 6(a), SEM images of TiO_2 electrode. The fabrication of a well defined TiO_2 nanostructure, with which has periodic hole arrays and a flat and dense TiO_2 film with a smooth surface is shown in Fig. 6(b) and (c), respectively. In case of 2D TiO_2 nanostructures, the pore diameter is ~90 nm and the depth of pore is same with thickness of TiO_2 (~100 nm). Here, the reason why we use ~90 nm scale structure, instead of 10 nm scale structure, is to improve the infiltration of polymers and this pore size and depth is very reproducible in our system. McGehee et al. reported the highest hole mobility of polymers incorporated into the straight nanopores of anodic alumina with the pore diameter of ~80 nm and Heeger et al. reported a very low incorporation of polymers of ~0.5%, even for highly porous TiO_2 nanocrystalline electrode [39,40]. Based on these reports, our 2D TiO_2 nanostructures can be considered as a good candidate for the hybrid solar cells.

The devices were constructed as shown in Fig. 7(a). As described above, a TiO_2 blocking layer was prepared on the ITO to prevent direct contact between the polymer and substrate, which results in a decrease in efficiency as the result of recombination. Three types of TiO_2 acceptor layers were then prepared followed by spin-coating of MEH-PPV and evaporation of Au as the electron donor and metal top electrode, respectively. As can be seen in the *I–V* curves shown in Fig. 7(b), an efficiency of 0.21% was obtained for the ordered 2D TiO_2 nanostructrue and MEH-PPV hybrid solar cells under one sun with air mass 1.5 global illumination without any optimization process of the metal electrode and annealing process, etc. However, the efficiencies of cells with the flat TiO_2 film and the random network

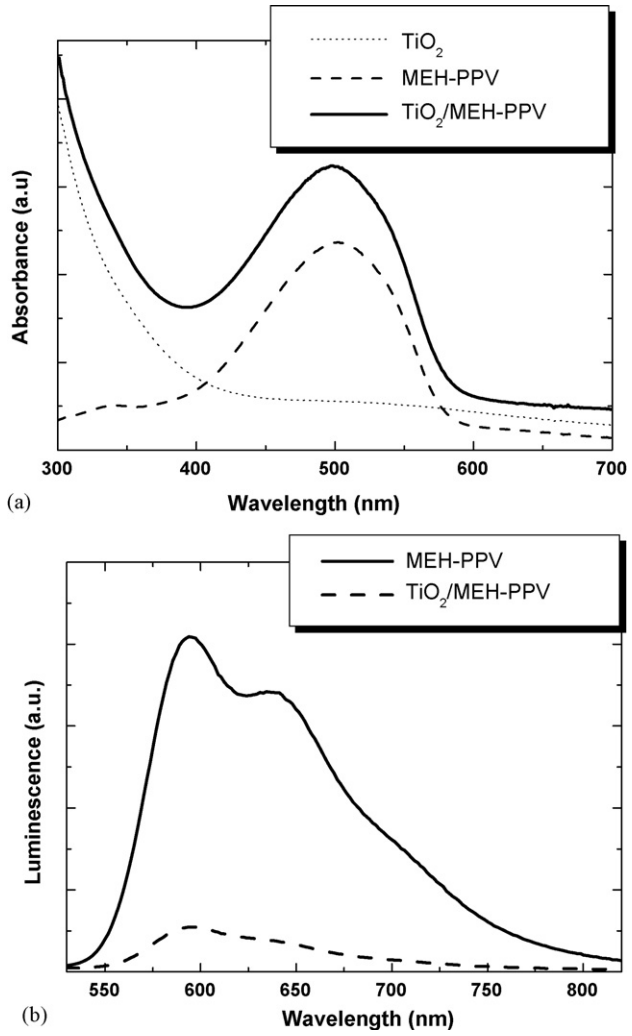

Fig. 5. (a) UV/vis absorption spectra of MEH-PPV, TiO_2, and TiO_2/MEH-PPV films and (b) PL spectra of MEH-PPV and TiO_2/MEH-PPV films.

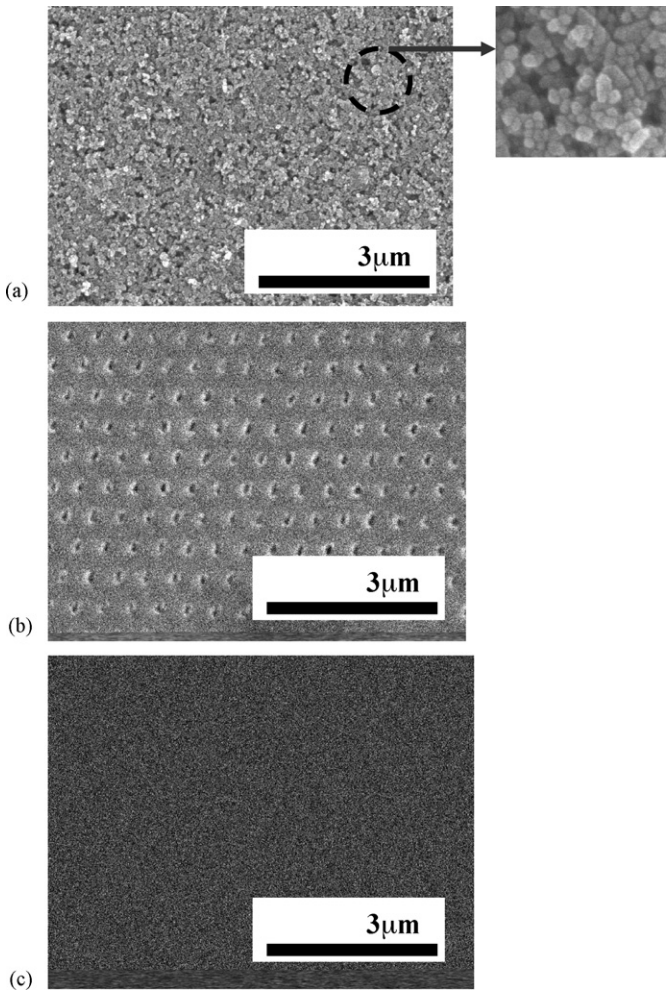

Fig. 6. SEM images of (a) a sintered random network of TiO_2 nanoparticles, (b) 2D TiO_2 nanostructures with hexagonal periodic hole arrays, and (c) a flat and dense TiO_2 film.

of sintered TiO_2 nanoparticles were estimated to 0.05 and 0.12%, respectively (see Table 1).

The highest and the lowest efficiency we obtained with 2D TiO_2 nanostructure was 0.25 and 0.19%, respectively. Usually, $0.21 \pm 0.02\%$ was obtained with almost constant V_{OC} and slightly changed FF. The variation in the FF can be attributed to the measurement conditions. These phenomena were also observed in the conventional random nanoparticle systems and thin-dense TiO_2 film system. Because we measure the performance in air, the FF can be slightly affected by the environment such as humidity. In our optical set-up and method, the formation of SRGs is very reproducible without any effect of environments such as humidity and temperature. Hence, the fabrication of nanostructures using these SRGs as templates can be considered to be a very easy and reproducible technique and similar efficiency value, which is one of the crucial requirements for practical device application can be obtained with this novel 2D TiO_2 structures.

Table 1
Photovoltaic characteristics of hybrid solar cells under the AM 1.5 illumination

	V_{OC} (V)	J_{SC} (mA/cm^2)	F.F (%)	((%)
Flat TiO_2 electrode	0.68	0.17	43.54	0.05
Random TiO_2 nanoparticle network	0.79	0.43	35.37	0.12
2D TiO_2 nanostructure	0.79	0.56	47.47	0.21

The performance of hybrid cells, specially photocurrent and fill factor, strongly depends on several factors including the amount of conjugated polymers, the absorption coefficient of polymers, interfacial area of TiO_2 and MEH-PPV, charge transport in the TiO_2 electrodes. Because MEH-PPV was spin-coated on three types of TiO_2 electrodes under the same conditions (same concentration of MEH-PPV in chlorobenzene, same speed and time), similar amount of MEH-PPV can be expected. The thickness of MEH-PPV on the substrate was evaluated to ~80 nm. For more accurate study, we compared the amount of MEH-PPV coated on three types of TiO_2 electrodes by measuring the UV/vis. absorption spectroscopy. Here, to remove the effect of TiO_2 electrodes, TiO_2/MEH-PPV films were immersed in the chlorobenzene to dissolve the MEH-PPV

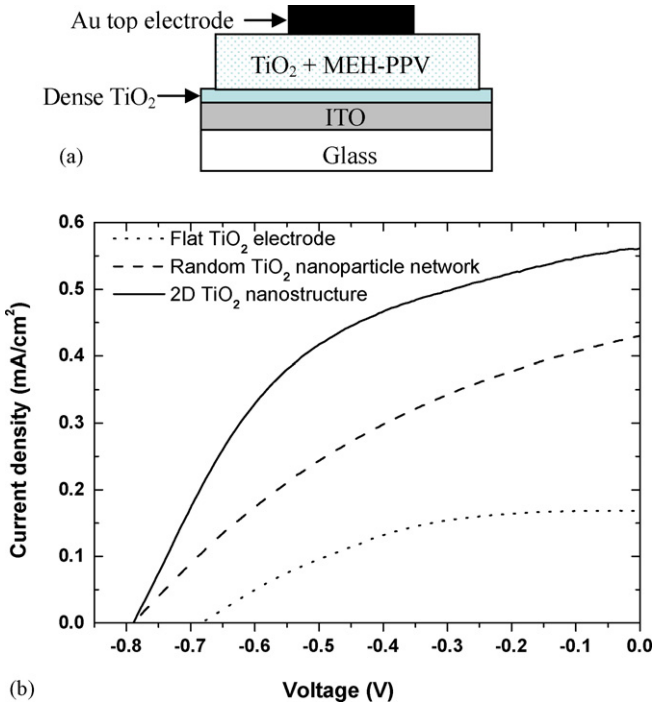

Fig. 7. (a) Schematic device structures and (b) *I–V* curves of hybrid solar cells with three types of TiO_2 acceptor layers.

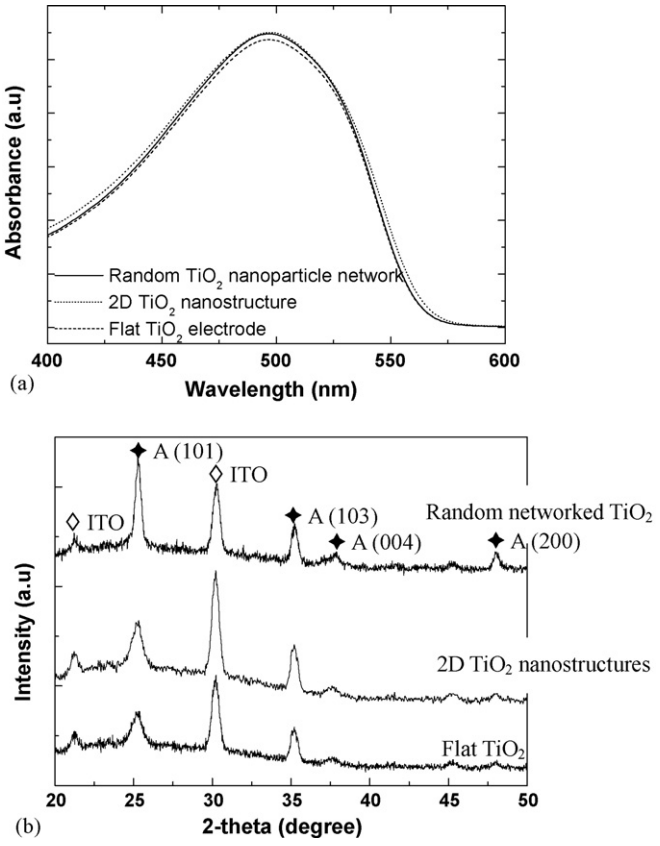

Fig. 8. (a) UV/vis absorption spectra of dissolve MEH-PPV solutions from three types of TiO_2 acceptor layers and (b) XRD diffraction patterns of three types of TiO_2 electrodes (♦: anatase TiO_2, ◊: ITO).

and then measured the UV/vis. absorption spectroscopy of that solution. Due to the similar absorbance shown in Fig. 8(a), the effect of the amount of MEH-PPV on performance can be ignored.

Another important factor, which determines the performance, is actual interfacial area of TiO_2 and MEH-PPV. Although real surface area of random networked TiO_2 nanoparticles is superior to that of the flat TiO_2 electrode and 2D TiO_2 nanostructures, relatively low interfacial area of TiO_2 and MEH-PPV can be expected due to the very poor incorporation of polymers to the random networked TiO_2 nanoparticles [39]. Considering very low interfacial area of flat TiO_2 and MEH-PPV, the lowest short-circuit current can be explained. In case of 2D TiO_2 nanostructures, because it has relatively high interfacial area due to the good incorporation of polymers to the holes with the diameter of ~90 nm and efficient charge transport resulted from the ordered electron accepting layers, the highest short-circuit current was found in the *I–V* measurement.

The crystallinity of electron accepting layer also has an influence on the electron transport. We prepared random networked TiO_2 nanocrystalline electrode by spin-coating the slurry of TiO_2 nanoparticles of ~15 nm followed by sintering at 425 °C. As shown in Fig. 8(b), it has sufficient crystallinity to transport the electron separated at the interface of TiO_2 and MEH-PPV. 2D TiO_2 nanostructures and flat TiO_2 electrode prepared by sol–gel reaction followed by sintering at 425 °C also shows polycrystalline nature. In the case of random networked TiO_2 nanoparticles, as mentioned above, the incorporation of MEH-PPV is very poor and randomly networked accepting layer results in the inefficient electron transport. Due to the poor electron transport resulted from the randomly networked accepting systems, the fill factor is relatively low and this phenomenon is general result in the randomly networked nanocrystalline system.

Compared to the limited charge transport in the electron accepting network which is formed by randomly interspersed nanocrystals, a more efficient charge separation and charge transport would be expected when a geometrical arrangement of the electron accepting network is achieved [16,17]. Improved electron transport can be explained indirectly through the measurement of A.C. impedance spectra, which give us the information about charge transfer resistance. Smaller circle was observed in the device with 2D TiO_2 nanostructures (not shown here). Which indicate decreased charge transfer resistance and efficient electron transport, resulting in the increase of fill factor and photocurrent.

Further optimization of this type of photovoltaic cells with smaller sized periodic hole arrays is currently underway.

4. Conclusions

The fabrication of ordered heterojunction organic–inorganic hybrid solar cells using well-ordered nanostructures of TiO_2 and MEH-PPV as an electron acceptor and donor, respectively, is described. The well-ordered TiO_2 nanostructure, which has periodic hexagonal hole arrays with a diameter of ~90 nm, was fabricated using 2D surface relief gratings on azobenzene-

functionalized polymer films as templates in the sol–gel reaction of a Ti-precusor. The efficiency was increased from 0.05 to 0.12%, for the flat TiO_2 film and random network of TiO_2 nanoparticles, to 0.21% using ordered 2D TiO_2 nanostructrues due to the relatively high interfacial area and more efficient charge separation and charge transport.

Acknowledgements

This work was financially supported by the Heeger Center for Advanced Materials (HCAM), National Research Laboratory (NRL) program of KOSEF, MOCIE (Ministry of Commerce, Industry and Energy, Korea), and Ministry of Education of Korea through BK21 program.

References

[1] N.S. Sariciftci, L. Smilowitz, A.J. Heeger, F. Wedl, Science 258 (1992) 1474.
[2] G. Yu, J. Gao, J.C. Hemmelen, F. Wudl, A.J. Heeger, Science 270 (1995) 1789.
[3] C.J. Brabec, N.S. Sariciftci, J.C. Hummelen, Adv. Funct. Mater. 11 (2001) 15.
[4] S. Alem, R.d. Bettignies, J.-M. Nunzi, M. Cariou, Appl. Phys. Lett. 84 (2004) 2178.
[5] V.D. Mihailetchi, L.J.A. Koster, P.W.M. Blom, Appl. Phys. Lett. 85 (2004) 970.
[6] X. Yang, J. Loos, S.C. Veenstra, W.J.N. Verhees, M.M. Wienk, J.M. Kroon, M.A.J. Michels, R.A.J. Janssen, Nano Lett. 5 (2005) 579.
[7] Y. Kim, S.A. Choulis, J. Nelson, D.D.C. Bradley, S. Cook, J.R. Durrant, Appl. Phys. Lett. 86 (2005) 063502.
[8] F. Padinger, R.S. Rittberger, N.S. Sariciftci, Adv. Funct. Mater. 13 (2003) 85.
[9] W. Ma, C. Yang, X. Gong, K. Lee, A.J. Heeger, Adv. Funct. Mater. 15 (2005) 1617.
[10] M. Reyes-Reyes, K. Kim, J. Dewald, R. López-Sandoval, A. Avadhanula, S. Curran, D.L. Carroll, Org. Lett. 7 (2005) 5749.
[11] G. Li, V. Shrotriya, J. Huang, Y. Yao, T. Moriarty, K. Emery, Y. Yang, Nat. Mater. 4 (2005) 864.
[12] A.C. Arango, S.A. Carter, P.J. Brock, Appl. Phys. Lett. 74 (1999) 1698.
[13] A.C. Arango, L.R. Johnson, V.N. Bliznyuk, Z. Schlesinger, S.A. Carter, H.-H. Hörhold, Adv. Mater. 12 (2000) 1689.
[14] A.J. Breeze, Z. Schlesinger, S.A. Carter, Phys. Rev. B 64 (2001), 125205-1.
[15] W.U. Huynh, J.J. Dittmer, A.P. Alivisatos, Science 295 (2002) 2425.
[16] K.M. Coakley, Y. Liu, M.D. McGehee, K.L. Frindell, G.D. Stucky, Adv. Funct. Mater. 13 (2003) 301.
[17] K.M. Coakley, M.D. McGehee, Appl. Phys. Lett. 83 (2003) 3380.
[18] M.Y. Song, J.K. Kim, K.-J. Kim, D.Y. Kim, Syn. Metal. 137 (2003) 1389.
[19] M.Y. Song, J.K. Kim, K.-J. Kim, D.Y. Kim, Syn. Metal. 137 (2003) 1387.
[20] L.H. Slooff, M.M. Wienk, J.M. Kroon, Thin Solid Films 451/452 (2004) 634.
[21] W.J.E. Beek, M.M. Wienk, R.A.J. Janssen, Adv. Mater. 16 (2004) 1009.
[22] W.J.E. Beek, L.H. Sloof, M.M. Wienk, J.M. Kroon, R.A.J. Janssen, Adv. Func. Mater. 15 (2005) 1703.
[23] D.C. Olson, J. Piris, R.T. Collins, S.E. Shaheen, D.S. Ginley, Thin Solid Films 496 (2006) 26.
[24] M. Lira-Cantu, F.C. Krebs, Sol. Energy Mater. Sol. Cells 90 (2006) 2076.
[25] Z. Xie, B.M. Henry, K.R. Kirov, H.E. Smith, A. Barkhouse, C.R.M. Grovenor, H.E. Assender, G.A.D. Briggs, G.R. Webster, P.L. Burn, M. Kano, Y. Tsukahara, Thin Solid Films 511/512 (2006) 523.
[26] H. Wang, C.C. Oey, A.B. Djurišić, M.H. Xie, Y.H. Leung, K.K.Y. Man, W.K. Chan, A. Pandey, J.-M. Nunzi, P.C. Chui, Appl. Phys. Lett. 87 (2005) 023507.
[27] C.C. Oey, A.B. Djurišić, H. Wang, K.K.Y. Man, W.K. Chan, M.H. Xie, Y.H. Leung, A. Pandey, J.-M. Nunzi, P.C. Chui, Nanotechnology 17 (2006) 706.
[28] P. Ravirajan, D.D.C. Bradely, J. Nelson, S.A. Haque, J.R. Durrand, H.J. Smit, J.M. Kroon, Appl. Phys. Lett. 86 (2005) 143101.
[29] M.Y. Song, K.-J. Kim, D.Y. Kim, Sol. Energy Mater. Sol. Cells 85 (2005) 31.
[30] D.Y. Kim, S.K. Tripathy, L. Li, J. Kumar, Appl. Phys. Lett. 66 (1995) 1166.
[31] P. Rochon, A. Natansohn, C.L. Callender, L. Robitaille, Appl. Phys. Lett. 71 (1997) 1008.
[32] J. Paterson, A. Natansohn, P. Rochon, C.L. Callender, L. Robitaille, Appl. Phys. Lett. 69 (1996) 3318.
[33] S. Bian, J.M. Williams, D.Y. Kim, L. Li, S. Balasubramanian, J. Kumar, S. Tripathy, Appl. Phys. Lett. 86 (1999) 4498.
[34] S.-S. Kim, C. Chun, J.-C. Hong, D.-Y. Kim, J. Mater. Chem. 16 (2006) 370.
[35] B.K. Mandal, R.J. Jeng, J. Kumar, S.K. Tripathy, Makromol. Chem., Rapid Commun. 12 (1991) 607.
[36] Q. Fan, B. McQuillin, D.D.C. Bradely, S. Whitelegg, A.B. Seddon, Chem. Phys. Lett. 347 (2001) 325.
[37] A. Petrella, M. Tamborra, M.L. Curri, P. Cosma, M. Striccoli, P.D. Cozzoli, A. Agostiano, J. Phys. Chem. B 109 (2005) 1554.
[38] N.C. Greenham, X. Peng, A.P. Alivisatos, Phys. Rev. B. 54 (1996) 17628.
[39] K.M. Coakley, B.S. Srinivasan, J.M. Ziebarth, C. Goh, Y. Liu, M.D. McGehee, Adv. Func. Mater. 15 (2005) 1927.
[40] G.P. Bartholomew, A.J. Heeger, Adv. Func. Mater. 15 (2005) 677.